

1 **Particle Phase State and Aerosol Liquid Water Greatly**
2 **Impact Secondary Aerosol Formation: Insights into Phase**
3 **Transition and Role in Haze Events**

4 Xiangxinyue Meng¹, Zhijun Wu^{1,2*}, Jingchuan Chen¹, Yanting Qiu¹, Taomou Zong¹,
5 Mijung Song³, Jiyi Lee⁴, Min Hu^{1,2}

6 1 State Key Joint Laboratory of Environmental Simulation and Pollution Control, International Joint
7 Laboratory for Regional Pollution Control, College of Environmental Sciences and Engineering, Peking
8 University, Beijing 100871, China

9 2 Collaborative Innovation Center of Atmospheric Environment and Equipment Technology, Nanjing
10 University of Information Science and Technology, Nanjing 210044, China

11 3 Department of Earth and Environmental Sciences, Jeonbuk National University, Jeonju, Republic of
12 Korea, 54896

13 4 Department of Environmental Science and Engineering, Ewha Womans University, Seoul, Republic of
14 Korea, 03760

15 **Corresponding author: zhijunwu@pku.edu.cn*

16 **Abstract.** The particle-phase state is crucial for reactive gas uptake, heterogeneous, and
17 multiphase chemical reactions, thereby impacting secondary aerosol formation. This
18 study provides valuable insights into the significance of particle-phase transition and
19 aerosol liquid water (ALW) in particle mass growth during winter. Our findings reveal
20 that particles predominantly exist as semi-solid or solid during clean winter days with
21 ambient relative humidity (RH) below 30%. However, non-liquid to liquid phase
22 transition occurs when the ALW mass fraction exceeds 15% (dry mass) at transition RH
23 thresholds of 40-60%. During haze episodes, the transformation rates of sulfate and
24 nitrate aerosols rapidly increase through phase transition and increased ALW by 48%
25 and 11%, respectively, resulting in noticeable increases in secondary inorganic aerosols
26 (SIA). The presence of abundant ALW, favored by elevated RH and higher proportion
27 of SIA, facilitates the partitioning of water-soluble compounds from gas to particle
28 phase, as well as heterogeneous and aqueous processes in liquid particles. This leads to

29 a substantial increase in the formation of secondary organic aerosols and elevated
30 aerosol oxidation. Consequently, the overall hygroscopicity parameters exhibit a
31 substantial enhancement with a mean value of 23%. These results highlight phase
32 transition as a key factor initiating the positive feedback loops between ALW and
33 secondary aerosol formation during haze episodes over the North China Plain. Accurate
34 predictions of secondary aerosol formation necessitate explicit consideration of the
35 particle-phase state in chemical transport models.

36 **1 Introduction**

37 Submicron particles are ubiquitous in the nature, having great impacts on climate,
38 visibility, and human health (Shiraiwa et al., 2011; Ravishankara, 1997; Pöschl,
39 2005; Lelieveld et al., 2015; Seinfeld et al., 2016; Hu et al., 2021). Phase state, a key
40 parameter of particles, plays profound roles in the mass transport of reactive molecules
41 between the gas phase and the particle phase (Marshall et al., 2018; Shiraiwa et al.,
42 2011). This, in turn, influences the gas-particle partitioning of semi-volatile materials
43 (Shiraiwa et al., 2013; Li and Shiraiwa, 2019), multiphase reaction rates of chemical
44 species (Zhang et al., 2018; Mu et al., 2018), and even the ice nucleating activities of
45 organic aerosols (OA) (Murray et al., 2010; Knopf and Alpert, 2023). Aerosol liquid
46 water (ALW) contributes a substantial fraction of the mass in sub-micrometer particles
47 on a global basis (Nguyen et al., 2016). Atmospheric particles with the presence of
48 condensed water serve as suspended vessels of multiphase chemical reactions, leading
49 to significant impacts on secondary aerosol formation, particle size growth, and air
50 quality (Wu et al., 2018; Hodas et al., 2014; Liu et al., 2019). Therefore, a comprehensive
51 understanding of particle-phase state and ALW is crucial for better evaluation of the
52 related environmental effects.

53 In the real atmosphere, the particle-phase state varies significantly among solid, semi-
54 solid, and liquid under different conditions, which specifically influenced by ambient
55 relative humidity (RH), temperature, and aerosol chemical composition. For example,
56 the atmospheric particles in the tropical rainforest over central Amazonia, which
57 primarily consisted of secondary organic aerosols (SOA) derived from oxidation of
58 isoprene, were observed to be in liquid state at $RH > 80\%$ (Bateman et al., 2016), but
59 more non-liquid particles occurred with the impact of anthropogenic pollutants
60 (Bateman et al., 2017). Liu et al. (2019) reported that particles with high mass fraction
61 of inorganics and high RH were prone to be liquid in a subtropical coastal megacity.
62 However, non-liquid particles appeared at $RH < 60\%$ in Beijing (Liu et al., 2017).
63 Moisture can drive an RH-induced glass transition in particles, leading to a liquid state

64 and a significant water uptake at high RH in the lower atmosphere (Mikhailov et al.,
65 2009). Moreover, organic aerosols might be in solid state at upper tropospheric
66 temperatures that below about 210 K (Koop et al., 2011). Therefore, the changing
67 features of aerosol composition and ambient RH may alter the ALW and trigger the
68 phase state variation. More studies are needed to clarify the relationship between
69 aerosol composition, particle-phase state, and ALW.

70 After the implementation of “China’s Action Plan for Air Pollution Prevention and
71 Control” in 2013, emissions of primary particulate matter and several gaseous
72 pollutants have greatly reduced. However, the contribution and proportion of secondary
73 inorganic aerosols (SIA) and secondary organic aerosols (SOA) have become
74 increasingly significant (Lei et al., 2021; Wang et al., 2021b), especially during haze
75 episodes in winter. As mentioned, particles changes from solid to liquid with elevated
76 RH conditions during heavy haze episodes (Liu et al., 2017). In liquid particles, the gas-
77 particle mass transfer for reactive gases can be greatly facilitated due to increased
78 diffusion coefficients, and the thermodynamic equilibrium of semi-volatile compounds
79 may be impacted to contribute to secondary aerosol formation (Shiraiwa et al., 2011; Jia
80 et al., 2023). A recent field study by Gkatzelis et al. (2021) pointed out that the gas-to-
81 particle partitioning in liquid particles enhances the uptake of water-soluble gas
82 compounds, resulting in a 15-25% contribution of SOA mass during particulate
83 pollution in Beijing. Many studies have demonstrated that the abundant ALW and high
84 RH condition can greatly impact secondary aerosol formation processes (Xu et al.,
85 2017; Wang et al., 2021a; Gkatzelis et al., 2021). However, there is still a lack of
86 understanding regarding the role of phase state variations in secondary particulate
87 pollution. In this study, we conducted a one-month field campaign in Beijing during
88 winter to investigate the relationship between particle-phase state, ALW, and the
89 chemical and physical processes involved in haze formation.

90 **2 Methodology**

91 **2.1 Instruments and Measurements**

92 Field campaigns were conducted in Beijing from 15th December 2020 to 10th January
93 2021 at the Changping campus of Peking University (40°8'N, 116°6'E). A detailed
94 description of the sampling site can be found in previous studies (Wang et al., 2020c).
95 The instruments were situated in the air monitoring laboratory, located on the top floor
96 of the main building. A weather station (Met One Instruments Inc., USA), a suite of
97 automatic gas analyzers (O₃, SO₂, CO and NO_x) from Thermo Scientific and an
98 Aerodyne Quadrupole Aerosol Chemical Speciation Monitor (Q-ACSM) were operated
99 according to standard protocols (Ng et al., 2011) and necessary information as described
100 in Text S1.

101 The particle rebound fraction (f) was measured using a modified three-arm impactor
102 (Bateman et al., 2014) coupled to a condensation particle counter (CPC, model 3772,
103 TSI Inc.) with a time interval of 3 minutes, as described in our previous work (Liu et
104 al., 2017; Meng et al., 2021). The three-arm impactor consisted of three parallel
105 impactors with different designs. One of the impactors had no plate, while the others
106 had plate equipped with an uncoated plate and a grease-coated plate, respectively. The
107 no-plate impactor provided the total throughput rate, while the solid surface of the
108 uncoated plate let particle rebound, and the sticky surface of the grease-coated plate
109 captured all particles that struck it. To measure the f , a valve system with three
110 solenoids and two actuators was used to ensure that the particle populations passing
111 through the three impactors were sequenced and were measured by the CPC. Thus,
112 rebound fraction, f , was defined as:

$$113 \quad f = \frac{N_2 - N_3}{N_1 - N_3} \quad (1)$$

114 where N_1 was the whole particle population, N_2 was the population of particles that did
115 not strike plus the rebounded particles from the impaction plate, and N_3 was the

116 population of particles that did not strike the impaction plate. Prior to measurement, we
117 dried the particles to below 30% RH using a silica gel diffusion dryer. Then, 300 nm
118 mono-disperse particles were selected by a Differential Mobility Analyzer (DMA, TSI
119 model 3080). An RH adjustment system with two RH probes and a Nafion RH
120 conditioner was employed to measure the RH conditions (ambient RH and impactor
121 RH), as well as to adjust the impactor RH to match the real atmospheric RH. The
122 measured impactor RH rapidly reached the ambient RH within 1 second, exhibiting a
123 mean absolute error of 0.03. This swift regulation time is attributed to the real-time
124 feedback in the RH control system, coupled with the typically modest fluctuations in
125 ambient RH. Particles with a diameter of 300 nm, as selected for our study, rapidly
126 achieved equilibrium in the humidification process, since the timescale for water
127 diffusion into these particles is approximately 1 second, shorter than their residence
128 time of about 3 seconds within the system. This is detailed in Text S2 and illustrated in
129 Figure S1. Such conditions ensure that the measured particle rebound are representative
130 and accurate at the ambient RH. Weekly calibrations using standard ammonium sulfate
131 and daily flow check were conducted (Liu et al., 2021;Liu et al., 2019). Typically, $f <$
132 0.2 or 0.1 are referred to the completely phase transition from non-liquid to liquid state
133 (Pajunoja et al., 2016;Liu et al., 2017). In this study, we consider $f < 0.2$ in the case of
134 liquid state. The time series of f with an initial time resolution is shown in Figure 1,
135 while the data presented in other figures are all displayed as hourly averages.

136 **2.2 Data Analysis**

137 The mass concentrations of organics, sulfate, nitrate, ammonium, and chloride in non-
138 refractory particles (NR-PM₁) were analyzed using the standard ACSM data analysis
139 software (v.1.5.10). A collection efficiency (CE) of 0.5 was applied to the dataset (Xu
140 et al., 2017;Matthew et al., 2008). Positive matrix factorization (PMF) was performed
141 on the organic mass spectra using the Igor Pro based PMF2.exe algorithm to resolve
142 primary organic aerosols (POA) and SOA factors. The data and error matrices were
143 pretreated following methods from previous studies (Zhang et al., 2011;Zhang et al.,

144 2017). The key diagnostic plots are provided in supplementary (Figure S2-S3).

145 The aerosol liquid water content contributed by inorganics (ALW_{inorg}) in PM_{10} was
146 estimated using the ISORROPIA-II thermodynamic model (Fountoukis and Nenes,
147 2007) with input of aerosol chemical composition measured by Q-ACSM. The particles
148 were assumed to be in metastable state, and the reverse mode was used to calculate the
149 ALW_{inorg} due to absence of gaseous HNO_3 and NH_3 . Besides, ALW associated with
150 organics (ALW_{org}) was considered using a simplified equation of k -Köhler theory (Guo
151 et al., 2015; Petters and Kreidenweis, 2007):

$$152 \quad ALW_{org} = V_{org} k_{org} \frac{a_w}{1-a_w}, \quad (2)$$

153 where V_{org} is the volume concentration of organics with a typical density of 1.4 g/cm^3
154 (Cerully et al., 2015), k_{org} is the hygroscopicity parameter of the organics, a_w represents
155 the water activity, which is assumed to have the same value as RH. In this study, we
156 used a fixed k_{org} of 0.06 to evaluate ALW_{org} , which was the average value of the overall
157 k_{org} in the consideration of POA and SOA contributions in the total non-refractory
158 organics ($k_{POA} = 0$ and $k_{SOA} = 0.1$) (Wu et al., 2016; Gunthe et al., 2011). However, it
159 should be noted that k_{org} has been found to exhibit a positive linear relationship with
160 the aerosol oxidation degree, which varied among species (Chang et al., 2010; Duplissy
161 et al., 2011). f_{44} , the fraction of m/z 44 fragment signal to total organic signal, is widely
162 used to represent the atmospheric aging process of OA species (Ng et al.,
163 2010; Canagaratna et al., 2015). Real-time k_{org} was $k_{org} = 1.04 \times f_{44} - 0.02$, as
164 reported by Kuang et al. (2020) for the North China Plain (NCP). The predicted real-
165 time k_{org} ranged from 0.13 to 0.24, which was consistent with the variation range
166 reported for winter Beijing (0.06-0.3) (Li et al., 2019; Jin et al., 2020). For fixed k_{org} ,
167 the contribution of organics to ALW was $\sim 12\%$ on average during the observation.
168 However, considering the variation of real-time f_{44} , organics were capable to provide
169 more than 30% and 20% of the total ALW mass on average during clean and polluted
170 days, respectively (Figure S4 and Text S3). In recognition of ALW's plasticizing effect

171 on particle-phase state, the potential impacts of whether the hygroscopicity value of
172 organics is fixed or varies in real-time on phase transition has been discussed in Section
173 3.2.

174 For a given internal mixture, the overall particle hygroscopicity (k_{total}) was calculated
175 by a simple mixing rule by weighting the hygroscopicity parameters of the components
176 by their volume fractions in the mixture (Petters and Kreidenweis, 2007):

$$177 \quad k_{total} = k_{inorg} \cdot frac_{inorg} + k_{org} \cdot frac_{org}, \quad (3)$$

178 Where $frac_{inorg}$ and $frac_{org}$ are the inorganics and organics volume fractions in NR-PM₁,
179 respectively. Considering the variability in the composition of inorganics and organics,
180 the hygroscopicity parameters of inorganics (k_{inorg}) was weighted by volume fractions.
181 The main form of inorganic species (NH₄NO₃ and (NH₄)₂SO₄) in the urban atmosphere
182 was considered due to the lower abundance of chloride in NR-PM₁. The volume fraction
183 of each inorganic species was calculated based on the ion-pairing scheme as described
184 in Gysel et al. (2007) with their gravimetric density (1720 kg m⁻³ for NH₄NO₃ and 1769
185 kg m⁻³ for (NH₄)₂SO₄) (Wu et al., 2016). The hygroscopicity parameters of NH₄NO₃
186 and (NH₄)₂SO₄ are 0.58 and 0.48, respectively following previous studies (Wu et al.,
187 2016;Jin et al., 2020;Petters and Kreidenweis, 2007). For hygroscopicity parameters of
188 organics (k_{org}), real-time k_{org} were used as above, which effectively captured the
189 characteristics of the investigated area in our study.

190 **3 Results and Discussion**

191 **3.1 Chemical Composition and Phase State of Sub-micrometer Particles**

192 Figure 1 shows the time series of meteorological parameters, chemical composition of
193 NR-PM₁, gas pollutants, and particle rebound fraction from December 16, 2020, to
194 January 10, 2021. The average mass concentration of NR-PM₁ was 15.8±16.8 µg m⁻³
195 during the measurement period. During clean periods (NR-PM₁ < 20 µg m⁻³), organics
196 dominated the aerosol composition, accounting for ~45% of NR-PM₁ mass. Nitrate,

197 sulfate, and ammonium contributed 20%, 16%, and 16% to total NR-PM₁ on average,
198 respectively (Figure S5). However, several pollution episodes occurred with rapid
199 growth in NR-PM₁ and ALW mass concentration with higher concentrations of NO_x
200 and SO₂, as marked by yellow shadow in Figure 1. These four polluted episodes
201 typically started with ambient RH below 40% and higher O₃ levels (> 30 ppb) and
202 mounted up with stagnant meteorological conditions bringing high RH (> 60% RH)
203 and low surface wind speed (< 3 m/s). This meteorological pattern is commonly
204 observed over the NCP during haze episodes (Sun et al., 2013; Sun et al., 2015). During
205 these polluted episodes, nitrate increased rapidly accounting for an average of 33% of
206 the total NR-PM₁ mass. ALW was minor during clean days, but increased up to 26% in
207 PM₁ during severe polluted episodes with NR-PM₁ > 80 μg m⁻³ (Figure S6). The mass
208 concentrations of POA and SOA both increased during these polluted episodes as
209 shown in Figure 1d. Moreover, the mass contribution of SOA to total OA showed an
210 upward trend in particulate mass, indicating the important contribution of secondary
211 formation during haze formation (Figure S7).

212 As shown in Figure 1f, particle rebound fraction, f , varied with ambient RH from 1.0 to
213 ~0.0 during the observation, indicating that particles possessed phase transition from
214 non-liquid to liquid state. Similar patterns of particle-phase transition were found for
215 several polluted episodes. Taking P4 as an example, f remained stable at 0.8 with RH =
216 ~20% during the initial period of stagnant conditions, but gradually dropped to ~0.1
217 along with the increasing RH and NR-PM₁ during the subsequent haze formation. In
218 addition, we collected several PM_{2.5} filter samples to characterize the bulk-phase
219 viscosity during clean and polluted days based on poke-and-flow experiment, as
220 described in our previous study (Song et al., 2022) and Text S4 (indicated by black and
221 red frames in Figure 1f). As shown in Figure S8, the viscosity was proved to be higher
222 than ~10⁸ Pa s with a mean value of $f > 0.8$ during clean days, indicating that particles
223 existed in a solid or semi-solid state. However, the viscosity was lower than ~10² Pa s
224 with an average $f < 0.2$ under higher RH conditions during polluted days, indicating the

225 liquid state. It should be noted that the viscosity measurement captured the bulk-phase
226 viscosity for water soluble components in PM_{2.5} filter samples, but the online
227 measurement of f depicted 300 nm particles representative of accumulation mode
228 particles, which normally contributed the majority fraction of PM₁. While the
229 differences in chemical composition between PM_{2.5} filter samples and 300 nm particles
230 may introduce uncertainties when comparing the phase state of the targeted aerosols,
231 the viscosity results showed good agreement with the average variation of f during the
232 corresponding period. Further validation is still necessary to compare the two different
233 techniques and will be displayed in our further study. To directly indicate the phase
234 transition from the perspective of viscosity, RH-dependent f was measured for these
235 filter samples with known bulk-phase viscosity (Figure S9 and Text S5). As expected,
236 the decreasing f from >0.8 to 0 covered the transition range from $\sim 10^8$ Pa s to $\sim 10^2$ Pa
237 s, which indicated the consistent behavior of particle rebound and measured bulk-phase
238 viscosity for the investigated aerosols.

239 **3.2 Phase Transition Behavior of Sub-micrometer Particles**

240 Figure 2a illustrates the frequency distribution of RH. f as a function of RH were plotted
241 in Figure 2b. During the observation, ambient RH was below 30% for more than half
242 of the time with f predominantly exceeding 0.8 under such conditions. When RH
243 increased to ~ 50 -60%, a majority of f dropped to <0.2 along with the increasing NR-
244 PM₁ mass. This means that particles went through a moisture-induced phase transition
245 from non-liquid to liquid during haze formation when RH reached 60%, which aligned
246 with our previous studies (Liu et al., 2017). Notably, some points with higher mass
247 fraction of inorganics ($f_{\text{inorg}} > 0.7$) showed $f < 0.2$ at RH = 40-50%, indicating that
248 particles with higher f_{inorg} were already in a liquid state. Consequently, particles
249 underwent phase transition with a relatively large RH range of 40-60%, exhibiting
250 varying chemical compositions as marked by the red frame.

251 Particle-phase state is known to be sensitive to ALW by its unique plasticizer effect

252 (Koop et al., 2011). In Figure 2d, f as a function of ALW/NR-PM₁ were plotted to
253 represent the relative water uptake of unit mass dry aerosols with corresponding particle
254 rebound behaviors. Figure 2c displays the frequency distribution of three f intervals in
255 each ALW/NR-PM₁ bin. When ALW/NR-PM₁ < 5%, the frequency of $f > 0.8$ was
256 higher than 0.65, indicating that particles mostly stay in a more viscous non-liquid state
257 with less water uptake capacity. When ALW/NR-PM₁ increased to 5-15%, f gradually
258 decreased from 0.8 to 0.2, suggesting that the total water uptake gradually enhanced
259 and lowered the viscosity to trigger the phase transition within this range. The non-
260 liquid particles were dominant with the frequency of $f=0.2-0.8$ close to 0.8. When
261 ALW/NR-PM₁ > 15%, the frequency of $f < 0.2$ dramatically increased from 0.2 to ~0.8,
262 reaching close to 1.0 at ALW/NR-PM₁ > 25% with higher particulate mass. This
263 indicates that particles mostly convert to liquid when the mass fraction of ALW
264 surpasses a certain threshold during haze formation, rather than the absolute ALW mass
265 (Figure S10). In general, a good correlation between ALW/NR-PM₁ and f was observed.
266 ALW/NR-PM₁, used as a mass-based hygroscopic growth factor (Chen et al., 2022; Liu
267 et al., 2018), is suitable to quantify the moisture-induced phase transition capacity of
268 atmospheric particles, and a value of 15% can be the sudden change in the case of phase
269 transition from non-liquid to liquid.

270 It should be noted that calculations of ALW in this study have considered inorganic
271 salts and organics. Acknowledging that the hygroscopicity of organics, characterized
272 by either a fixed k_{org} or varying in real-time, affects the calculation of ALW mass, a
273 sensitivity analysis examining its impact on the phase transition threshold (ALW/NR-
274 PM₁) is presented in Figure S11. There is no denying that the contribution of inorganic
275 salts to ALW remains predominant, with their contribution to ALW being ~88% (a fixed
276 k_{org} of 0.06) and ~73.5% (real-time k_{org}) on average during the observation (Figure S4),
277 indicating that the impact of different ALW calculations on ALW/NR-PM₁ values was
278 minor. As expected, the frequency distribution of these three f intervals showed no
279 obvious change for ALW calculations by inorganics, fixed k_{org} , and real-time k_{org} at the

280 whole ALW/NR-PM₁ range. Although the frequency of $f < 0.2$ changed from ~ 0.8 to
281 0.5 at ALW/NR-PM₁ = 15-20% when shifting to real-time k_{org} , the frequency remained
282 higher than 0.5 and approached 1.0 with larger ALW/NR-PM₁ values. This indicates
283 that while the varying k_{org} impacts the number of data points within ALW/NR-PM₁ bins
284 of 15-20%, it does not affect the overall transition trend. As a result, the impacts of
285 different ALW calculation on ALW/NR-PM₁ were not significant, and the phase
286 transition threshold of 15% remains valid. It is suggested that caution should be
287 exercised when using the above approach to characterize the phase state of targeted
288 aerosols, as the measured f was representative of accumulation mode particles that
289 dominated the mass concentration of submicron particles (Seinfeld, 2006).

290 It is interesting to note that several points with ALW/NR-PM₁ < 5% and NR-PM₁ > 30
291 $\mu\text{g}/\text{m}^3$ exhibited lower rebound fraction ($f < 0.4$), which was attributed to the variation
292 of RH background from high RH to low RH during the later stages of the haze episodes,
293 as shown in Figure 2d and Figure S12. This suggests that liquid particles may not turn
294 to be a more viscous semi-solid state in a brief period under dehydration process. There
295 are two possible explanations for this phenomenon. Firstly, the presence of significant
296 amounts of inorganic and organic compounds can alter the humidity conditions for
297 deliquescence and efflorescence (Ushijima et al., 2021; Peckhaus et al., 2012). Secondly,
298 these particles are likely become non-ideal mixing due to drying process that form core-
299 shell structure (Shiraiwa et al., 2013; Ciobanu et al., 2009; Song et al., 2013). Studies
300 have revealed that outer phase may form viscous organic shell to prevent water
301 evaporation (Koop et al., 2011; Shiraiwa et al., 2013; Hodas et al., 2015), thus, the inner
302 phase containing inorganics still keep liquid with residual water. However, it should be
303 noted that liquid-liquid phase separation was not optically detected under staged
304 dehydration of filter-based Beijing PM_{2.5} droplets by Song et al. (2022). Instead, they
305 observed abrupt effloresced inorganics at $\sim 30\%$ RH, which was much lower than
306 $(\text{NH}_4)_2\text{SO}_4$ and NH_4NO_3 in pure form (Peng et al., 2022). This supports that
307 atmospheric particles are more likely to be metastable after liquification only if RH

308 decreases to very low values.

309 In addition to RH and aerosol compositions, environmental temperature also plays a
310 significant role in determining the phase state (Koop et al., 2011; Shiraiwa et al.,
311 2017; Petters et al., 2019). A reduction in temperature results in higher viscosity,
312 whereas a rise in RH leads to a decrease in viscosity, attributed to the plasticizing effect
313 of water (Koop et al., 2011). Although the relationship between f and temperature is not
314 strongly evident as that of RH in this study (Figure S13), it's observed that a greater
315 number of data points exhibited near 0.9 under low RH conditions (<30%), suggesting
316 higher viscosity at colder temperatures (< -10 °C) than warmer scenarios. The glass
317 transition temperature (T_g) is a key metric for the non-equilibrium phase transition from
318 a glassy solid to a semi-solid state as temperature rises (Koop et al., 2011). Particles act
319 as solid when the temperature falls below T_g ($T_g/T > 1$), and transition to semi-solid or
320 liquid at temperature exceeding T_g . An increase in compound molecular weight, O:C
321 ratio, and functional group composition are identified as key factors affecting the T_g of
322 OA (Saukko et al., 2012; Dette et al., 2014; Rothfuss and Petters, 2017; Shiraiwa et al.,
323 2017). Shiraiwa et al (2017) proposed that T_g/T is an indicator for the semi-solid to
324 liquid phase transition of OA, with a threshold of $T_g/T \approx 0.8$. In this study, we employed
325 a T_g parameterization method for OA viscosity based on their molecular weight and
326 O:C ratio to assess the combined effects of aerosol composition, RH and temperature
327 on particle phase state (Shiraiwa et al., 2017). This method accounts for water
328 associated with both inorganics and organics, rather than focusing solely on organics,
329 to calculate T_g of ambient OA, as elaborated in Text S6.

330 Figure 3a displays the characteristic relations between T_g/T and ALW/NR-PM₁ with
331 different approach for T_g calculations of ambient OA. Different phase state intervals are
332 characterized by T_g/T based on predicted viscosity η as shown in Figure 3b, and are
333 illustrated using dashed lines with arrows. The predicted viscosity η of OA was
334 calculated by applying the Vogel–Tammann–Fulcher (VTF) equation (Angell, 1991)
335 with a fragility parameter of 10 (DeRieux et al., 2018). Clearly, after calculating T_g in

336 conjunction with k_{total} , there is a strong consistency in the characteristic relationship
337 between the estimated T_g/T and ALW/NR-PM₁ with both fixed and variable k_{org} . This
338 consistency aligns well with the phase state changes of atmospheric aerosols discussed
339 earlier in this study. In contrast, even when accounting for variations in hygroscopicity
340 due to different oxidation degrees of OA, the majority of these estimated T_g/T values
341 fall within the semi-solid and solid range at higher ALW/NR-PM₁, significantly
342 deviating from the field observations. This highlights the significant impact of
343 environmental RH and chemical composition on the moisture-induced phase transition
344 of atmospheric particles in the near-surface atmosphere. In particular, inorganic salts
345 play a dominant role, contributing more significantly to the mass fraction of ALW in
346 total particulate matter. The estimated T_g/T for ambient OA with k_{total} transitioned to a
347 liquid state at ALW/NR-PM₁ > 10%, which is slightly lower than the transition
348 threshold of 15% proposed in this study. It should be noted that the estimated T_g of OA
349 adopted an average molecular weight (MW) of 200 g mol⁻¹, as used in previous studies
350 (Williams et al., 2010; Shen et al., 2018). However, the average MW of ambient OA is
351 likely variable due to the atmospheric aging process. Increasing the value of MW can
352 shift the characteristic curve of T_g/T versus ALW/NR-PM₁ to the right, thereby aligning
353 the semi-solid to liquid transition threshold more closely with the results observed in
354 this study. This further suggests that incorporating of k_{total} into T_g calculation may
355 potentially enhance the simulation results, especially in regions with a high proportion
356 of inorganic salts under humid conditions. It should be noted that this aspect warrants
357 further exploration in subsequent research.

358 **3.3 Effects of Phase Transition and ALW on SIA Formation during Haze Episodes**

359 We investigated the f and secondary aerosols during four polluted episodes (P1 to P4)
360 under stagnant weather conditions with WS < 3 ms⁻¹. Sulfur and nitrogen oxidation
361 ratios, SOR ($nSO_4/(nSO_4 + nSO_2)$) and NOR ($nNO_3/(nNO_3 + nNO_2)$), commonly
362 used as indicators for secondary inorganic transformation (Li et al., 2017), are plotted
363 as a function of f in Figure 4a and 4b. We found that SOR (NOR) remained in a lower

364 level with a mean value of ~ 0.27 (0.08) at $f > 0.2$ for non-liquid particles, but increased
365 significantly to ~ 0.8 (0.35) with increasing ALW/NR-PM₁ at $f < 0.2$. This indicates that
366 the secondary formation of SIA is facilitated to a certain degree through phase transition
367 and the increasingly higher ALW mass. It should be noted that particles can be non-
368 liquid during haze episodes with $f = 1.0-0.2$. Interestingly, SOR and NOR remained in
369 lower levels and did not show notable increase between $f = 1.0-0.8$ and $f = 0.8-0.2$, until
370 particles accomplished the phase transition at $f = 0.2-0.0$ (Figure 4c1 and 4c2). As a
371 result, the median SOR (NOR) increased to higher levels with an increment of 48%
372 (11%) via phase transition along with the increase in ALW.

373 From the perspective of phase state, the increasing mass fraction of ALW reduces the
374 viscosity and triggers the phase transition, which have important roles in the gas-
375 particle mass transfer during haze formation. It is suggested that the secondary
376 transformation of SIA is impeded by limited mass transfer between gas and particle
377 phase when particles are not fully converted into liquid state. However, these limited
378 factors disappear or the dominant formation pathway changes after phase transition. As
379 reported in previous studies, ALW facilitates the secondary formation of sulfate and
380 nitrate via the promotion of heterogeneous reactions (e.g. SO₂ heterogeneous oxidation,
381 N₂O₅ hydrolysis), gas-particle partitioning of semi-volatile components or aqueous-
382 phase reactions on wet aerosols (Chen et al., 2022; Cheng et al., 2016; Wang et al.,
383 2020b; Liu et al., 2020). However, aqueous-phase oxidation of SO₂ may be constrained
384 before phase transition due to the low diffusivity of multiple oxidants (e.g. O₃, H₂O₂
385 and NO₂) in the particles, and it may become the dominant formation pathway in liquid
386 particles (Ravishankara, 1997; Liu et al., 2020). Additionally, the partitioning of nitrate
387 into particles following Henry's Law may also be facilitated by the increased ALW due
388 to enhanced diffusivity of dissolved precursors in liquid particles. In Figure 4d, the mass
389 fraction of SIA ($f_{\text{SIA/NR-PM}_1}$) is plotted as a function of f . The $f_{\text{SIA/NR-PM}_1}$, ALW mass
390 concentration, and RH were grouped and averaged corresponding to f bin width of 10%.
391 We found that $f_{\text{SIA/NR-PM}_1}$ remained stable at $f = 1.0-0.4$, but steadily increased from an

392 average of ~ 0.50 to ~ 0.65 with elevated RH levels ($>40\%$) and decreasing f (from 0.4
393 to 0.0). This indicates that SIA formation was limited for non-liquid particles with
394 higher viscosity under lower RH conditions. However, ALW was steadily enhanced by
395 the increasing RH and started to trigger the phase transition, thereby facilitating the
396 SOR and NOR to a larger extent. Therefore, $f_{\text{SIA/NR-PM}_1}$ apparently increased with the
397 increase in ALW at $f = 0.2-0.0$. The presence of more ALW in liquid particles was
398 expected to promote the SIA formation by acting as multiphase reaction vessels (Zheng
399 et al., 2015; Wang et al., 2020a; Wang et al., 2020b). One should note that, the average
400 environmental temperature during pollution episodes increased to approximately 0°C ,
401 in contrast to the -10°C recorded during clean periods. The rise in ambient temperature
402 typically enhances the diffusivity of atmospheric reactive molecules in both the gas and
403 particle phases (Tang et al., 2014; Shiraiwa et al., 2011; Li and Shiraiwa, 2019). This, in
404 turn, may potentially influence the heterogeneous or liquid-phase reactions, and even
405 the gas-particle partitioning of semi-volatile compounds.

406 **3.4 Effects of Phase Transition and ALW on SOA Formation during Haze Episodes**

407 In Figure 5a and 5b, the ratio of SOA to POA (SOA/POA) is plotted as a function of f
408 during these four polluted episodes characterized by ALW/NR-PM₁ and f_{44} . For $f = 1.0-$
409 0.2 , particles possessed relatively lower SOA/POA values (1-2.5) with ALW/NR-PM₁
410 $<15\%$, which was independent of NR-PM₁ mass concentrations. However, a noticeable
411 increase in SOA/POA and elevated f_{44} values were observed at $f = 0.2-0.0$, accompanied
412 by increasing ALW/NR-PM₁ and NR-PM₁ mass. This indicates that more oxidized SOA
413 was produced in liquid particles through the phase transition and the increasing mass
414 fraction of ALW during haze formation. Interestingly, we observed that these liquid
415 particles were primarily associated with polluted days during the nighttime (Figure
416 S14). For these liquid particles, SOA/POA doubled to ~ 5.5 along with the increasing
417 f_{44} compared to non-liquid particles, suggesting the important roles of phase transition
418 and ALW in promoting the SOA formation through dark reactions during nighttime.
419 From the perspective of phase state, phase transition was directly indicated by the

420 decreasing f during haze formation driving a large decrease in bulk phase viscosity
421 from $>10^8$ Pa s to $<10^2$ Pa s as proved by viscosity measurement, which may enhance
422 the gas-particle mass transfer. ALW reduces the viscosity and triggers the phase
423 transition, thus facilitating the uptake of precursors and oxidants, and potentially
424 altering the reaction pathway (Tillmann et al., 2010; Berkemeier et al., 2016; Li et al.,
425 2018; Zhao et al., 2019).

426 For non-liquid particles, ALW facilitates the SOA formation via partition and
427 heterogeneous uptake of water-soluble organics from gas phase into the particle phase,
428 leading to a rapid increase in SOA along with ALW (Herrmann et al., 2015; Gkatzelis
429 et al., 2021; Lim et al., 2010; El-Sayed et al., 2015). Subsequent aqueous-phase reactions
430 may occur to form oligomers, organosulfates, and nitrogen-containing organics through
431 radical or non-radical reactions (Surratt et al., 2007; Iinuma et al., 2007; Galloway et al.,
432 2009; Lim et al., 2013; Wang et al., 2020c). However, these reactions may be limited in
433 non-liquid particles by the lower diffusivity due to higher viscosity. In contrast, liquid
434 particles provide unstrained mass transfer of necessary oxidants and precursors between
435 gas and particle phase, which is favorable for aqueous-phase processing. It is well
436 known that aqueous-phase processing can contribute more oxidized SOA (Xu et al.,
437 2017; Ervens et al., 2011; Zheng et al., 2023). Recent field studies have demonstrated
438 that oligomers or dicarboxylic acids were enriched in liquid particles from the reactive
439 uptake of methylglyoxal during the severe haze episodes in Beijing (Zheng et al., 2021).
440 These oxidation products formed through aqueous-phase reactions are typically more
441 oxidized and less volatile than those formed through gas phase photochemistry (Ervens
442 et al., 2011), which can be reserved in the particle phase and increased the SOA mass
443 in total OA. Therefore, the significant growth of SOA/POA and f_{44} after phase transition
444 is attributed by the enhanced heterogeneous or aqueous-phase reactions in liquid
445 particles with abundant ALW during the nighttime.

446 3.5 Positive Feedback Loops between ALW and Secondary Aerosol Formation 447 Triggered by Phase Transition during Haze Episodes

448 In Figure 6a, the relationship between the overall particle hygroscopicity (k_{total}) and RH
449 is displayed. The k_{total} , ALW, and NR-PM₁ mass were grouped and averaged
450 corresponding to an RH bin width of 10%. When RH was below 30%, the averaged
451 k_{total} was ~0.35. However, it increased to 0.39 with higher ALW and NR-PM₁ mass at
452 RH =40-60%, and further rose to 0.43 with an average maximum NR-PM₁ value of 56
453 $\mu\text{g}/\text{m}^3$ when RH reached 70-80%. This indicates that hygroscopic growth of particulate
454 matter underwent two stages with increasing RH and NR-PM₁ mass, particularly at RH
455 = 40-60% and RH > 70%. From the above discussion, we have demonstrated that the
456 non-liquid to liquid phase transition was triggered by the increased ALW, with a
457 transition RH threshold of 40-60% during haze episodes (as indicated by gradual color
458 change in Figure 6a). Phase transition facilitated the formation of sulfate and nitrate
459 aerosols, contributing higher proportion of SIA in total particles under higher RH
460 conditions. Notably, this led to a continuous increase in the volume fraction of
461 inorganics with increasing RH (Figure 6b). Besides, k_{inorg} also slightly increased when
462 RH reached 60% due to increased nitrate contribution in total SIA during haze episodes
463 (Figure 6c and Figure S5). This may explain the first enhancement of k_{total} at RH = 40-
464 60%, which was mainly driven by the large increase in $frac_{inorg}$ favored by phase
465 transition.

466 Furthermore, the increase in k_{total} , coupled with elevated RH levels, led to a greater
467 abundance of ALW mass. Heterogeneous or aqueous-phase reactions were favored with
468 increasing ALW, promoting the formation of more oxidized SOA in liquid particles. At
469 RH > 70%, the significant increase in k_{org} (~14%) compensated for the negative effect
470 of decreased $frac_{org}$ on the total hygroscopicity contributed by organics ($k_{org} \cdot frac_{org}$),
471 leading to a stable $k_{org} \cdot frac_{org}$ with increasing RH (Figure 6c and Figure S15). This, in
472 turn, coordinated with the increased $frac_{inorg}$, resulting in the second enhancement of

473 k_{total} . As a result, phase transition accompanied by increasing ALW mass triggered a
474 noticeable enhancement in k_{total} with a mean value of 23% during haze episodes. The
475 enhanced water uptake ability of aerosols is expected to contribute more ALW under
476 elevated RH conditions, further facilitating the secondary aerosol formation and
477 deteriorating air quality. These results indicate that the establishment of positive
478 feedback loops between ALW and secondary aerosol formation was triggered by phase
479 transition during haze episodes.

480 **4 Conclusion and atmospheric implications**

481 Our findings revealed that particles predominantly exist as semi-solid or solid during
482 clean winter days with RH below 30%. However, non-liquid to liquid phase transition
483 occurred when the ALW mass fraction surpassed 15% (dry mass) at transition RH
484 thresholds ranging from 40% to 60%. Additionally, we observed a consistent pattern in
485 the non-liquid to liquid phase transition during haze formation, as manifested by both
486 particle-rebound fraction and bulk-phase viscosity measurements. Specifically, the
487 decrease in f from >0.8 to 0 corresponded to a viscosity transition ranging from $\sim 10^8$
488 Pa s to $\sim 10^2$ Pa s. With the incorporation of k_{total} into T_g calculation for ambient OA, we
489 found that the characteristic of T_g/T versus ALW/NR-PM₁ agrees well with our field
490 observations. This finding offers insights into the effectiveness of ALW/NR-PM₁ as an
491 indicator for quantifying the moisture-induced phase transition capacity of atmospheric
492 particles. Furthermore, incorporating overall particle hygroscopicity into the T_g
493 calculation may potentially enhance OA viscosity simulations, especially in regions
494 with a high proportion of inorganic salts under humid conditions. During haze episodes,
495 SOR and NOR rapidly increased through phase transition and increased ALW by 48%
496 and 11%, respectively, resulting in noticeable increases in SIA. The presence of
497 abundant ALW, favored by elevated RH and higher proportion of SIA, facilitates
498 heterogeneous and aqueous processes in liquid particles, leading to a substantial
499 increase in the formation of secondary organic aerosols and elevated aerosol oxidation.
500 As a result, the overall hygroscopicity parameters exhibit a substantial enhancement

501 with a mean value of 23%.

502 In our previous studies, we have revealed the positive feedback loops between ALW
503 and anthropogenic SIA at elevated RH levels during haze formation (Wu et al.,
504 2018;Wang et al., 2020b). The contribution of abundant ALW to SOA production has
505 also been reported in various regions with active anthropogenic emissions, such as the
506 Po Valley in Italy, southeastern U.S., and Beijing, China (Carlton and Turpin,
507 2013;Hodas et al., 2014;Xu et al., 2017). However, we observed that secondary
508 transformation of SIA and SOA was significantly enhanced after phase transition with
509 higher ALW mass during the observation. Our findings indicate that the secondary
510 aerosol formation could be impeded on non-liquid particles due to limited mass transfer
511 between gas and particle phase for relevant reaction components (Ravishankara,
512 1997;Shiraiwa et al., 2011;Abbatt et al., 2012;Ma et al., 2022), whereas it is facilitated
513 in liquid particles. It is therefore recommended that non-liquid to liquid phase transition
514 may be considered to be the kick-off for the positive feedback loops between ALW and
515 secondary aerosol formation during haze events. This can be further supported by the
516 case studies for varying polluted episodes, where episodes with phase transition
517 generally exhibit higher secondary transformation rate of secondary aerosols compared
518 to episodes without phase transition (Figure S16 and Text S7). This mechanism is
519 expected to gain significance in other regions with abundant anthropogenic emissions
520 and high background RH during haze formation.

521 **Author contributions**

522 X.X.Y.M. and Z.J.W. conceived the study. X.X.Y.M. conducted the experiments,
523 analyzed the experimental data, and wrote the manuscript with contributions from
524 Z.J.W., M.J.S., J.Y.L. and M.H. J.C.C. participated in the offline experiments and data
525 analysis. Y.T.Q. and T.M.Z. participated in the field experiments and conducted the
526 filter sampling.

527 **Funding**

528 This work was supported by the National Natural Science Foundation of China (Grant No.
529 42375093) and the Fine Particle Research Initiative in East Asia Considering National Differences
530 (FRIEND) Project through the National Research Foundation of Korea (NRF:
531 2020M3G1A1114537) funded by the Ministry of Science and ICT, Korea.

532 **Data availability**

533 The data presented in this article can be accessed through the corresponding author Zhijun Wu
534 (zhijunwu@pku.edu.cn).

535 **Acknowledgments**

536 We sincerely thank our two referees for their valuable comments and constructive suggestions to
537 improve the scientific and rigorous nature of our manuscript. We gratefully acknowledge the
538 assistance of Wenfei Zhu for the technical support on Q-ACSM running and instrument calibration
539 during the campaign.

540 **Competing interests**

541 The authors declare that they have no conflict of interest.

542 **Reference**

- 543 Abbatt, J. P. D., Lee, A. K. Y., and Thornton, J. A.: Quantifying trace gas uptake to tropospheric
544 aerosol: recent advances and remaining challenges, *Chem. Soc. Rev.*, 41, 6555–6581, 2012.
- 545 Angell, C. A.: Relaxation in Liquids, Polymers and Plastic Crystals - Strong Fragile Patterns and
546 Problems, *J Non-Cryst Solids*, 131, 13–31, 1991.
- 547 Bateman, A. P., Belassein, H., and Martin, S. T.: Impactor Apparatus for the Study of Particle
548 Rebound: Relative Humidity and Capillary Forces, *Aerosol Sci. Technol.*, 48, 42–52,
549 10.1080/02786826.2013.853866, 2014.
- 550 Bateman, A. P., Gong, Z. H., Liu, P. F., Sato, B., Cirino, G., Zhang, Y., Artaxo, P., Bertram, A. K., Manzi,
551 A. O., Rizzo, L. V., Souza, R. A. F., Zaveri, R. A., and Martin, S. T.: Sub-micrometre particulate matter
552 is primarily in liquid form over Amazon rainforest, *Nat. Geosci.*, 9, 34–+, 2016.
- 553 Bateman, A. P., Gong, Z. H., Harder, T. H., de Sa, S. S., Wang, B. B., Castillo, P., China, S., Liu, Y. J.,
554 O'Brien, R. E., Palm, B. B., Shiu, H. W., Cirino, G. G., Thalman, R., Adachi, K., Alexander, M. L., Artaxo,
555 P., Bertram, A. K., Buseck, P. R., Gilles, M. K., Jimenez, J. L., Laskin, A., Manzi, A. O., Sedlacek, A.,
556 Souza, R. A. F., Wang, J., Zaveri, R., and Martin, S. T.: Anthropogenic influences on the physical
557 state of submicron particulate matter over a tropical forest, *Atmos. Chem. Phys.*, 17, 1759–1773,
558 2017.
- 559 Berkemeier, T., Steimer, S. S., Krieger, U. K., Peter, T., Pöschl, U., Ammann, M., and Shiraiwa, M.:

560 Ozone uptake on glassy, semi-solid and liquid organic matter and the role of reactive oxygen
561 intermediates in atmospheric aerosol chemistry, *Phys. Chem. Chem. Phys.*, 18, 12662-12674,
562 10.1039/C6CP00634E, 2016.

563 Canagaratna, M. R., Jimenez, J. L., Kroll, J. H., Chen, Q., Kessler, S. H., Massoli, P., Hildebrandt Ruiz,
564 L., Fortner, E., Williams, L. R., Wilson, K. R., Surratt, J. D., Donahue, N. M., Jayne, J. T., and Worsnop,
565 D. R.: Elemental ratio measurements of organic compounds using aerosol mass spectrometry:
566 characterization, improved calibration, and implications, *Atmos. Chem. Phys.*, 15, 253-272,
567 10.5194/acp-15-253-2015, 2015.

568 Carlton, A. G., and Turpin, B. J.: Particle partitioning potential of organic compounds is highest in
569 the Eastern US and driven by anthropogenic water, *Atmos. Chem. Phys.*, 13, 10203-10214,
570 10.5194/acp-13-10203-2013, 2013.

571 Cerully, K. M., Bougiatioti, A., Hite Jr, J. R., Guo, H., Xu, L., Ng, N. L., Weber, R., and Nenes, A.: On
572 the link between hygroscopicity, volatility, and oxidation state of ambient and water-soluble
573 aerosols in the southeastern United States, *Atmos. Chem. Phys.*, 15, 8679-8694, 10.5194/acp-15-
574 8679-2015, 2015.

575 Chang, R. Y. W., Slowik, J. G., Shantz, N. C., Vlasenko, A., Liggio, J., Sjostedt, S. J., Leaitch, W. R., and
576 Abbatt, J. P. D.: The hygroscopicity parameter (κ) of ambient organic aerosol at a field site subject
577 to biogenic and anthropogenic influences: relationship to degree of aerosol oxidation, *Atmos.*
578 *Chem. Phys.*, 10, 5047-5064, 10.5194/acp-10-5047-2010, 2010.

579 Chen, Y., Wang, Y., Nenes, A., Wild, O., Song, S. J., Hu, D. W., Liu, D. T., He, J. J., Ruiz, L. H., Apte, J.
580 S., Gunthe, S. S., and Liu, P. F.: Ammonium Chloride Associated Aerosol Liquid Water Enhances
581 Haze in Delhi, India, *Environ. Sci. Technol.*, 56, 7163-7173, 10.1021/acs.est.2c00650, 2022.

582 Cheng, Y., Zheng, G., Wei, C., Mu, Q., Zheng, B., Wang, Z., Gao, M., Zhang, Q., He, K., Carmichael,
583 G., Pöschl, U., and Su, H.: Reactive nitrogen chemistry in aerosol water as a source of sulfate during
584 haze events in China, *Sci. Adv.*, 2, e1601530, doi:10.1126/sciadv.1601530, 2016.

585 Ciobanu, V. G., Marcolli, C., Krieger, U. K., Weers, U., and Peter, T.: Liquid-Liquid Phase Separation
586 in Mixed Organic/Inorganic Aerosol Particles, *J. Phys. Chem. A*, 113, 10966-10978, 2009.

587 DeRieux, W. S., Li, Y., Lin, P., Laskin, J., Laskin, A., Bertram, A. K., Nizkorodov, S. A., and Shiraiwa, M.:
588 Predicting the glass transition temperature and viscosity of secondary organic material using
589 molecular composition, *Atmos Chem Phys*, 18, 6331-6351, 2018.

590 Dette, H. P., Qi, M., Schröder, D. C., Godt, A., and Koop, T.: Glass-Forming Properties of 3-
591 Methylbutane-1,2,3-tricarboxylic Acid and Its Mixtures with Water and Pinonic Acid, *The Journal*
592 *of Physical Chemistry A*, 118, 7024-7033, 10.1021/jp505910w, 2014.

593 Duplissy, J., DeCarlo, P. F., Dommen, J., Alfarra, M. R., Metzger, A., Barmapadimos, I., Prevot, A. S.
594 H., Weingartner, E., Tritscher, T., Gysel, M., Aiken, A. C., Jimenez, J. L., Canagaratna, M. R., Worsnop,
595 D. R., Collins, D. R., Tomlinson, J., and Baltensperger, U.: Relating hygroscopicity and composition
596 of organic aerosol particulate matter, *Atmos. Chem. Phys.*, 11, 1155-1165, 10.5194/acp-11-1155-
597 2011, 2011.

598 El-Sayed, M. M. H., Wang, Y. Q., and Hennigan, C. J.: Direct atmospheric evidence for the
599 irreversible formation of aqueous secondary organic aerosol, *Geophys. Res. Lett.*, 42, 5577-5586,
600 10.1002/2015gl064556, 2015.

601 Ervens, B., Turpin, B. J., and Weber, R. J.: Secondary organic aerosol formation in cloud droplets
602 and aqueous particles (aqSOA): a review of laboratory, field and model studies, *Atmos. Chem.*

603 Phys., 11, 11069-11102, 10.5194/acp-11-11069-2011, 2011.

604 Fountoukis, C., and Nenes, A.: ISORROPIA II: a computationally efficient thermodynamic
605 equilibrium model for K^+ - Ca^{2+} - Mg^{2+} - NH_4^+ - Na^+ - SO_4^{2-} - NO_3^- - Cl^- - H_2O aerosols, *Atmos.*
606 *Chem. Phys.*, 7, 4639-4659, DOI 10.5194/acp-7-4639-2007, 2007.

607 Galloway, M. M., Chhabra, P. S., Chan, A. W. H., Surratt, J. D., Flagan, R. C., Seinfeld, J. H., and
608 Keutsch, F. N.: Glyoxal uptake on ammonium sulphate seed aerosol: reaction products and
609 reversibility of uptake under dark and irradiated conditions, *Atmos. Chem. Phys.*, 9, 3331-3345,
610 10.5194/acp-9-3331-2009, 2009.

611 Gkatzelis, G. I., Papanastasiou, D. K., Karydis, V. A., Hohaus, T., Liu, Y., Schmitt, S. H., Schlag, P.,
612 Fuchs, H., Novelli, A., Chen, Q., Cheng, X., Broch, S., Dong, H., Holland, F., Li, X., Liu, Y. H., Ma, X. F.,
613 Reimer, D., Rohrer, F., Shao, M., Tan, Z., Taraborrelli, D., Tillmann, R., Wang, H. C., Wang, Y., Wu, Y.
614 S., Wu, Z. J., Zeng, L. M., Zheng, J., Hu, M., Lu, K. D., Hofzumahaus, A., Zhang, Y. H., Wahner, A.,
615 and Kiendler-Scharr, A.: Uptake of Water-soluble Gas-phase Oxidation Products Drives Organic
616 Particulate Pollution in Beijing, *Geophys. Res. Lett.*, 48, ARTN e2020GL091351
617 10.1029/2020GL091351, 2021.

618 Gunthe, S. S., Rose, D., Su, H., Garland, R. M., Achtert, P., Nowak, A., Wiedensohler, A., Kuwata, M.,
619 Takegawa, N., Kondo, Y., Hu, M., Shao, M., Zhu, T., Andreae, M. O., and Pöschl, U.: Cloud
620 condensation nuclei (CCN) from fresh and aged air pollution in the megacity region of Beijing,
621 *Atmos. Chem. Phys.*, 11, 11023-11039, 10.5194/acp-11-11023-2011, 2011.

622 Guo, H., Xu, L., Bougiatioti, A., Cerully, K. M., Capps, S. L., Hite Jr, J. R., Carlton, A. G., Lee, S. H.,
623 Bergin, M. H., Ng, N. L., Nenes, A., and Weber, R. J.: Fine-particle water and pH in the southeastern
624 United States, *Atmos. Chem. Phys.*, 15, 5211-5228, 10.5194/acp-15-5211-2015, 2015.

625 Gysel, M., Crosier, J., Topping, D. O., Whitehead, J. D., Bower, K. N., Cubison, M. J., Williams, P. I.,
626 Flynn, M. J., McFiggans, G. B., and Coe, H.: Closure study between chemical composition and
627 hygroscopic growth of aerosol particles during TORCH2, *Atmos Chem Phys*, 7, 6131-6144, 2007.

628 Herrmann, H., Schaefer, T., Tilgner, A., Styler, S. A., Weller, C., Teich, M., and Otto, T.: Tropospheric
629 Aqueous-Phase Chemistry: Kinetics, Mechanisms, and Its Coupling to a Changing Gas Phase,
630 *Chem. Rev.*, 115, 4259-4334, 10.1021/cr500447k, 2015.

631 Hodas, N., Sullivan, A. P., Skog, K., Keutsch, F. N., Collett, J. L., Decesari, S., Facchini, M. C., Carlton,
632 A. G., Laaksonen, A., and Turpin, B. J.: Aerosol Liquid Water Driven by Anthropogenic Nitrate:
633 Implications for Lifetimes of Water-Soluble Organic Gases and Potential for Secondary Organic
634 Aerosol Formation, *Environ. Sci. Technol.*, 48, 11127-11136, 2014.

635 Hodas, N., Zuend, A., Mui, W., Flagan, R. C., and Seinfeld, J. H.: Influence of particle-phase state
636 on the hygroscopic behavior of mixed organic-inorganic aerosols, *Atmos. Chem. Phys.*, 15, 5027-
637 5045, 10.5194/acp-15-5027-2015, 2015.

638 Hu, S. Y., Zhao, G., Tan, T. Y., Li, C. C., Zong, T. M., Xu, N., Zhu, W. F., and Hu, M.: Current challenges
639 of improving visibility due to increasing nitrate fraction in PM_{2.5} during the haze days in Beijing,
640 China, *Environ. Pollut.*, 290, 2021.

641 Iinuma, Y., Müller, C., Berndt, T., Boge, O., Claeys, M., and Herrmann, H.: Evidence for the existence
642 of organosulfates from beta-pinene ozonolysis in ambient secondary organic aerosol, *Environ. Sci.*
643 *Technol.*, 41, 6678-6683, 10.1021/es070938t, 2007.

644 Jia, L., Xu, Y., and Duan, M.: Explosive formation of secondary organic aerosol due to aerosol-fog

645 interactions, *Sci. Total Environ.*, 866, 161338, <https://doi.org/10.1016/j.scitotenv.2022.161338>,
646 2023.

647 Jin, X., Wang, Y., Li, Z., Zhang, F., Xu, W., Sun, Y., Fan, X., Chen, G., Wu, H., Ren, J., Wang, Q., and
648 Cribb, M.: Significant contribution of organics to aerosol liquid water content in winter in Beijing,
649 China, *Atmos. Chem. Phys.*, 20, 901-914, 10.5194/acp-20-901-2020, 2020.

650 Knopf, D. A., and Alpert, P. A.: Atmospheric ice nucleation, *Nat Rev Phys*, 5, 203-217,
651 10.1038/s42254-023-00570-7, 2023.

652 Koop, T., Bookhold, J., Shiraiwa, M., and Poschl, U.: Glass transition and phase state of organic
653 compounds: dependency on molecular properties and implications for secondary organic aerosols
654 in the atmosphere, *Phys. Chem. Chem. Phys.*, 13, 19238-19255, 10.1039/c1cp22617g, 2011.

655 Kuang, Y., He, Y., Xu, W., Zhao, P., Cheng, Y., Zhao, G., Tao, J., Ma, N., Su, H., Zhang, Y., Sun, J.,
656 Cheng, P., Yang, W., Zhang, S., Wu, C., Sun, Y., and Zhao, C.: Distinct diurnal variation in organic
657 aerosol hygroscopicity and its relationship with oxygenated organic aerosol, *Atmos. Chem. Phys.*,
658 20, 865-880, 10.5194/acp-20-865-2020, 2020.

659 Lei, L., Zhou, W., Chen, C., He, Y., Li, Z. J., Sun, J. X., Tang, X., Fu, P. Q., Wang, Z. F., and Sun, Y. L.:
660 Long-term characterization of aerosol chemistry in cold season from 2013 to 2020 in Beijing, China,
661 *Environ. Pollut.*, 268, 2021.

662 Lelieveld, J., Evans, J. S., Fnais, M., Giannadaki, D., and Pozzer, A.: The contribution of outdoor air
663 pollution sources to premature mortality on a global scale, *Nature*, 525, 367-371,
664 10.1038/nature15371, 2015.

665 Li, X. X., Song, S. J., Zhou, W., Hao, J. M., Worsnop, D. R., and Jiang, J. K.: Interactions between
666 aerosol organic components and liquid water content during haze episodes in Beijing, *Atmos.*
667 *Chem. Phys.*, 19, 12163-12174, 2019.

668 Li, Y., and Shiraiwa, M.: Timescales of secondary organic aerosols to reach equilibrium at various
669 temperatures and relative humidities, *Atmos. Chem. Phys.*, 19, 5959-5971, 10.5194/acp-19-5959-
670 2019, 2019.

671 Li, Y. J., Sun, Y., Zhang, Q., Li, X., Li, M., Zhou, Z., and Chan, C. K.: Real-time chemical
672 characterization of atmospheric particulate matter in China: A review, *Atmos. Environ.*, 158, 270-
673 304, <https://doi.org/10.1016/j.atmosenv.2017.02.027>, 2017.

674 Li, Z., Smith, K. A., and Cappa, C. D.: Influence of relative humidity on the heterogeneous oxidation
675 of secondary organic aerosol, *Atmos. Chem. Phys.*, 18, 14585-14608, 10.5194/acp-18-14585-
676 2018, 2018.

677 Lim, Y. B., Tan, Y., Perri, M. J., Seitzinger, S. P., and Turpin, B. J.: Aqueous chemistry and its role in
678 secondary organic aerosol (SOA) formation, *Atmos. Chem. Phys.*, 10, 10521-10539, 10.5194/acp-
679 10-10521-2010, 2010.

680 Lim, Y. B., Tan, Y., and Turpin, B. J.: Chemical insights, explicit chemistry, and yields of secondary
681 organic aerosol from OH radical oxidation of methylglyoxal and glyoxal in the aqueous phase,
682 *Atmos. Chem. Phys.*, 13, 8651-8667, 10.5194/acp-13-8651-2013, 2013.

683 Liu, P., Song, M., Zhao, T., Gunthe, S. S., Ham, S., He, Y., Qin, Y. M., Gong, Z., Amorim, J. C., Bertram,
684 A. K., and Martin, S. T.: Resolving the mechanisms of hygroscopic growth and cloud condensation
685 nuclei activity for organic particulate matter, *Nat. Commun.*, 9, 4076, 10.1038/s41467-018-06622-
686 2, 2018.

687 Liu, T., Clegg, S. L., and Abbatt, J. P. D.: Fast oxidation of sulfur dioxide by hydrogen peroxide in

688 deliquesced aerosol particles, *Proc. Natl. Acad. Sci. U.S.A.* , 117, 1354-1359,
689 doi:10.1073/pnas.1916401117, 2020.

690 Liu, Y., Wu, Z., Wang, Y., Xiao, Y., Gu, F., Zheng, J., Tan, T., Shang, D., Wu, Y., Zeng, L., Hu, M.,
691 Bateman, A. P., and Martin, S. T.: Submicrometer Particles Are in the Liquid State during Heavy
692 Haze Episodes in the Urban Atmosphere of Beijing, China, *Environ. Sci. Technol. Lett.* , 4, 427-432,
693 10.1021/acs.estlett.7b00352, 2017.

694 Liu, Y., Wu, Z., Huang, X., Shen, H., Bai, Y., Qiao, K., Meng, X., Hu, W., Tang, M., and He, L.: Aerosol
695 Phase State and Its Link to Chemical Composition and Liquid Water Content in a Subtropical
696 Coastal Megacity, *Environ. Sci. Technol.* , 53, 5027-5033, 10.1021/acs.est.9b01196, 2019.

697 Liu, Y. C., Meng, X. X., Wu, Z. J., Huang, D. D., Wang, H. L., Chen, J., Chen, J. C., Zong, T. M., Fang,
698 X., Tan, T. Y., Zhao, G., Chen, S. Y., Zeng, L. W., Guo, S., Huang, X. F., He, L. Y., Zeng, L. M., and Hu,
699 M.: The particle phase state during the biomass burning events, *Sci. Total Environ.*, 792, ARTN
700 148035
701 10.1016/j.scitotenv.2021.148035, 2021.

702 Ma, W., Zheng, F. X., Zhang, Y. S., Chen, X., Zhan, J. L., Hua, C. J., Song, B. Y., Wang, Z. C., Xie, J. L.,
703 Yan, C., Kulmala, M., and Liu, Y. C.: Weakened Gas-to-Particle Partitioning of Oxygenated Organic
704 Molecules in Liquefied Aerosol Particles, *Environ. Sci. Technol. Lett.*, 10.1021/acs.estlett.2c00556,
705 2022.

706 Marshall, F. H., Berkemeier, T., Shiraiwa, M., Nandy, L., Ohm, P. B., Dutcher, C. S., and Reid, J. P.:
707 Influence of particle viscosity on mass transfer and heterogeneous ozonolysis kinetics in aqueous-
708 sucrose-maleic acid aerosol, *Phys. Chem. Chem. Phys.*, 20, 15560-15573, 2018.

709 Matthew, B. M., Middlebrook, A. M., and Onasch, T. B.: Collection efficiencies in an Aerodyne
710 Aerosol Mass Spectrometer as a function of particle phase for laboratory generated aerosols,
711 *Aerosol Sci. Technol.*, 42, 884-898, 10.1080/02786820802356797, 2008.

712 Meng, X. X. Y., Wu, Z. J., Guo, S., Wang, H., Liu, K. F., Zong, T. M., Liu, Y. C., Zhang, W. B., Zhang,
713 Z., Chen, S. Y., Zeng, L. M., Hallquist, M., Shuai, S. J., and Hu, M.: Humidity-Dependent Phase State
714 of Gasoline Vehicle Emission-Related Aerosols, *Environ. Sci. Technol.* , 55, 832-841, 2021.

715 Mikhailov, E., Vlasenko, S., Martin, S. T., Koop, T., and Poschl, U.: Amorphous and crystalline aerosol
716 particles interacting with water vapor: conceptual framework and experimental evidence for
717 restructuring, phase transitions and kinetic limitations, *Atmos. Chem. Phys.*, 9, 9491-9522, 2009.

718 Mu, Q., Shiraiwa, M., Octaviani, M., Ma, N., Ding, A. J., Su, H., Lammel, G., Poschl, U., and Cheng, Y.
719 F.: Temperature effect on phase state and reactivity controls atmospheric multiphase chemistry
720 and transport of PAHs, *Sci. Adv.*, 4, 2018.

721 Murray, B. J., Wilson, T. W., Dobbie, S., Cui, Z. Q., Al-Jumur, S. M. R. K., Mohler, O., Schnaiter, M.,
722 Wagner, R., Benz, S., Niemand, M., Saathoff, H., Ebert, V., Wagner, S., and Karcher, B.:
723 Heterogeneous nucleation of ice particles on glassy aerosols under cirrus conditions, *Nat. Geosci.*,
724 3, 233-237, 2010.

725 Ng, N. L., Canagaratna, M. R., Zhang, Q., Jimenez, J. L., Tian, J., Ulbrich, I. M., Kroll, J. H., Docherty,
726 K. S., Chhabra, P. S., Bahreini, R., Murphy, S. M., Seinfeld, J. H., Hildebrandt, L., Donahue, N. M.,
727 DeCarlo, P. F., Lanz, V. A., Prevot, A. S. H., Dinar, E., Rudich, Y., and Worsnop, D. R.: Organic aerosol
728 components observed in Northern Hemispheric datasets from Aerosol Mass Spectrometry, *Atmos.*
729 *Chem. Phys.*, 10, 4625-4641, 10.5194/acp-10-4625-2010, 2010.

730 Ng, N. L., Herndon, S. C., Trimborn, A., Canagaratna, M. R., Croteau, P. L., Onasch, T. B., Sueper, D.,
731 Worsnop, D. R., Zhang, Q., Sun, Y. L., and Jayne, J. T.: An Aerosol Chemical Speciation Monitor
732 (ACSM) for Routine Monitoring of the Composition and Mass Concentrations of Ambient Aerosol,
733 *Aerosol Sci. Technol.*, 45, 780-794, Pii 934555189

734 10.1080/02786826.2011.560211, 2011.

735 Nguyen, T. K. V., Zhang, Q., Jimenez, J. L., Pike, M., and Carlton, A. G.: Liquid Water: Ubiquitous
736 Contributor to Aerosol Mass, *Environ. Sci. Technol. Lett.*, 3, 257-263, 2016.

737 Pajunoja, A., Hu, W. W., Leong, Y. J., Taylor, N. F., Miettinen, P., Palm, B. B., Mikkonen, S., Collins,
738 D. R., Jimenez, J. L., and Virtanen, A.: Phase state of ambient aerosol linked with water uptake and
739 chemical aging in the southeastern US, *Atmos. Chem. Phys.*, 16, 11163-11176, 2016.

740 Peckhaus, A., Grass, S., Treuel, L., and Zellner, R.: Deliquescence and Efflorescence Behavior of
741 Ternary Inorganic/Organic/Water Aerosol Particles, *J. Phys. Chem. A*, 116, 6199-6210,
742 10.1021/jp211522t, 2012.

743 Peng, C., Chen, L. X. D., and Tang, M. J.: A database for deliquescence and efflorescence relative
744 humidities of compounds with atmospheric relevance, *Fund Res-China*, 2, 578-587,
745 10.1016/j.fmre.2021.11.021, 2022.

746 Petters, M. D., and Kreidenweis, S. M.: A single parameter representation of hygroscopic growth
747 and cloud condensation nucleus activity, *Atmos. Chem. Phys.*, 7, 1961-1971, 2007.

748 Petters, S. S., Kreidenweis, S. M., Grieshop, A. P., Ziemann, P. J., and Petters, M. D.: Temperature-
749 and Humidity-Dependent Phase States of Secondary Organic Aerosols, *Geophys Res Lett*, 46,
750 1005-1013, <https://doi.org/10.1029/2018GL080563>, 2019.

751 Pöschl, U.: Atmospheric Aerosols: Composition, Transformation, Climate and Health Effects,
752 *Angewandte Chemie International Edition*, 44, 7520-7540,
753 <https://doi.org/10.1002/anie.200501122>, 2005.

754 Ravishankara, A. R.: Heterogeneous and multiphase chemistry in the troposphere, *Science*, 276,
755 1058-1065, 1997.

756 Rothfuss, N. E., and Petters, M. D.: Influence of Functional Groups on the Viscosity of Organic
757 Aerosol, *Environmental Science & Technology*, 51, 271-279, 10.1021/acs.est.6b04478, 2017.

758 Saukko, E., Lambe, A. T., Massoli, P., Koop, T., Wright, J. P., Croasdale, D. R., Pedernera, D. A.,
759 Onasch, T. B., Laaksonen, A., Davidovits, P., Worsnop, D. R., and Virtanen, A.: Humidity-dependent
760 phase state of SOA particles from biogenic and anthropogenic precursors, *Atmos Chem Phys*, 12,
761 7517-7529, 2012.

762 Seinfeld, J. H., Bretherton, C., Carslaw, K. S., Coe, H., DeMott, P. J., Dunlea, E. J., Feingold, G., Ghan,
763 S., Guenther, A. B., Kahn, R., Kraucunas, I., Kreidenweis, S. M., Molina, M. J., Nenes, A., Penner, J. E.,
764 Prather, K. A., Ramanathan, V., Ramaswamy, V., Rasch, P. J., Ravishankara, A. R., Rosenfeld, D.,

765 Stephens, G., and Wood, R.: Improving our fundamental understanding of the role of aerosol-
766 cloud interactions in the climate system, *Proc. Natl. Acad. Sci. U. S. A.*, 113, 5781-5790,
767 doi:10.1073/pnas.1514043113, 2016.

768 Seinfeld, J. H., and Pandis, S. N.: *Atmospheric Chemistry and Physics: From Air Pollution to Climate*
769 *Change*, Wiley, 2006.

770 Shen, H., Chen, Z., Li, H., Qian, X., Qin, X., and Shi, W.: Gas-Particle Partitioning of Carbonyl

771 Compounds in the Ambient Atmosphere, *Environmental Science & Technology*, 52, 10997-11006,
772 10.1021/acs.est.8b01882, 2018.

773 Shiraiwa, M., Ammann, M., Koop, T., and Poschl, U.: Gas uptake and chemical aging of semisolid
774 organic aerosol particles, *Proc. Natl. Acad. Sci. U. S. A.*, 108, 11003-11008,
775 10.1073/pnas.1103045108, 2011.

776 Shiraiwa, M., Zuend, A., Bertram, A. K., and Seinfeld, J. H.: Gas-particle partitioning of atmospheric
777 aerosols: interplay of physical state, non-ideal mixing and morphology, *Phys. Chem. Chem. Phys.*,
778 15, 11441-11453, 2013.

779 Shiraiwa, M., Li, Y., Tsimpidi, A. P., Karydis, V. A., Berkemeier, T., Pandis, S. N., Lelieveld, J., Koop, T.,
780 and Poschl, U.: Global distribution of particle phase state in atmospheric secondary organic
781 aerosols, *Nature Communications*, 8, 2017.

782 Song, M., Jeong, R., Kim, D., Qiu, Y., Meng, X., Wu, Z., Zuend, A., Ha, Y., Kim, C., Kim, H., Gaikwad,
783 S., Jang, K.-S., Lee, J. Y., and Ahn, J.: Comparison of Phase States of PM_{2.5} over Megacities, Seoul
784 and Beijing, and Their Implications on Particle Size Distribution, *Environ. Sci. Technol.* ,
785 10.1021/acs.est.2c06377, 2022.

786 Song, M. J., Marcolli, C., Krieger, U. K., Lienhard, D. M., and Peter, T.: Morphologies of mixed
787 organic/inorganic/aqueous aerosol droplets, *Faraday Discuss.*, 165, 289-316, 2013.

788 Sun, Y. L., Wang, Z. F., Fu, P. Q., Yang, T., Jiang, Q., Dong, H. B., Li, J., and Jia, J. J.: Aerosol
789 composition, sources and processes during wintertime in Beijing, China, *Atmos. Chem. Phys.*, 13,
790 4577-4592, 10.5194/acp-13-4577-2013, 2013.

791 Sun, Y. L., Du, W., Wang, Q. Q., Zhang, Q., Chen, C., Chen, Y., Chen, Z. Y., Fu, P. Q., Wang, Z. F.,
792 Gao, Z. Q., and R., W. D.: Real-Time Characterization of Aerosol Particle Composition above the
793 Urban Canopy in Beijing: Insights into the Interactions between the Atmospheric Boundary Layer
794 and Aerosol Chemistry, *Environ. Sci. Technol.* , 2015 v.49 no.19, pp. 11340-11347,
795 10.1021/acs.est.5b02373, 2015.

796 Surratt, J. D., Kroll, J. H., Kleindienst, T. E., Edney, E. O., Claeys, M., Sorooshian, A., Ng, N. L.,
797 Offenberg, J. H., Lewandowski, M., Jaoui, M., Flagan, R. C., and Seinfeld, J. H.: Evidence for
798 organosulfates in secondary organic aerosol, *Environ. Sci. Technol.*, 41, 517-527,
799 10.1021/es062081q, 2007.

800 Tang, M. J., Cox, R. A., and Kalberer, M.: Compilation and evaluation of gas phase diffusion
801 coefficients of reactive trace gases in the atmosphere: volume 1. Inorganic compounds, *Atmos.*
802 *Chem. Phys.*, 14, 9233-9247, 10.5194/acp-14-9233-2014, 2014.

803 Tillmann, R., Hallquist, M., Jonsson, Å. M., Kiendler-Scharr, A., Saathoff, H., Iinuma, Y., and Mentel,
804 T. F.: Influence of relative humidity and temperature on the production of pinonaldehyde and OH
805 radicals from the ozonolysis of α -pinene, *Atmos. Chem. Phys.*, 10, 7057-7072, 10.5194/acp-
806 10-7057-2010, 2010.

807 Ushijima, S. B., Huynh, E., Davis, R. D., and Tolbert, M. A.: Seeded Crystal Growth of Internally Mixed
808 Organic-Inorganic Aerosols: Impact of Organic Phase State, *J. Phys. Chem. A*, 125, 8668-8679,
809 10.1021/acs.jpca.1c04471, 2021.

810 Wang, H., Chen, X., Lu, K., Tan, Z., Ma, X., Wu, Z., Li, X., Liu, Y., Shang, D., Wu, Y., Zeng, L., Hu, M.,
811 Schmitt, S., Kiendler-Scharr, A., Wahner, A., and Zhang, Y.: Wintertime N₂O₅ uptake coefficients
812 over the North China Plain, *Sci. Bull.*, 65, 765-774, <https://doi.org/10.1016/j.scib.2020.02.006>,
813 2020a.

814 Wang, J. F., Ye, J. H., Zhang, Q., Zhao, J., Wu, Y. Z., Li, J. Y., Liu, D. T., Li, W. J., Zhang, Y. G., Wu, C.,
815 Xie, C. H., Qin, Y. M., Lei, Y. L., Huang, X. P., Guo, J. P., Liu, P. F., Fu, P. Q., Li, Y. J., Lee, H. C., Choi,
816 H., Zhang, J., Liao, H., Chen, M. D., Sun, Y. L., Ge, X. L., Martin, S. T., and Jacob, D. J.: Aqueous
817 production of secondary organic aerosol from fossil-fuel emissions in winter Beijing haze, *Proc.*
818 *Natl. Acad. Sci. U.S.A.* , 118, 2021a.

819 Wang, Y., Chen, Y., Wu, Z. J., Shang, D. J., Bian, Y. X., Du, Z. F., Schmitt, S. H., Su, R., Gkatzelis, G. I.,
820 Schlag, P., Hohaus, T., Voliotis, A., Lu, K. D., Zen, L. M., Zhao, C. S., Alfarra, M. R., McFiggans, G.,
821 Wiedensohler, A., Kiendler-Scharr, A., Zhang, Y. H., and Hu, M.: Mutual promotion between aerosol
822 particle liquid water and particulate nitrate enhancement leads to severe nitrate-dominated
823 particulate matter pollution and low visibility, *Atmos. Chem. Phys.*, 20, 2161-2175, 2020b.

824 Wang, Y., Hu, M., Wang, Y.-C., Li, X., Fang, X., Tang, R., Lu, S., Wu, Y., Guo, S., Wu, Z., Hallquist, M.,
825 and Yu, J. Z.: Comparative Study of Particulate Organosulfates in Contrasting Atmospheric
826 Environments: Field Evidence for the Significant Influence of Anthropogenic Sulfate and NO_x,
827 *Environ. Sci. Technol. Lett.*, 7, 787-794, 10.1021/acs.estlett.0c00550, 2020c.

828 Wang, Y. Y., Li, Z. Q., Wang, Q. Y., Jin, X. A., Yan, P., Cribb, M., Li, Y. A., Yuan, C., Wu, H., Wu, T.,
829 Ren, R. M., and Cai, Z. X.: Enhancement of secondary aerosol formation by reduced anthropogenic
830 emissions during Spring Festival 2019 and enlightenment for regional PM_{2.5} control in Beijing,
831 *Atmos. Chem. Phys.*, 21, 915-926, 2021b.

832 Williams, B. J., Goldstein, A. H., Kreisberg, N. M., and Hering, S. V.: In situ measurements of
833 gas/particle-phase transitions for atmospheric semivolatile organic compounds, *Proceedings of*
834 *the National Academy of Sciences*, 107, 6676-6681, doi:10.1073/pnas.0911858107, 2010.

835 Wu, Z. J., Zheng, J., Shang, D. J., Du, Z. F., Wu, Y. S., Zeng, L. M., Wiedensohler, A., and Hu, M.:
836 Particle hygroscopicity and its link to chemical composition in the urban atmosphere of Beijing,
837 China, during summertime, *Atmos. Chem. Phys.*, 16, 1123-1138, 10.5194/acp-16-1123-2016,
838 2016.

839 Wu, Z. J., Wang, Y., Tan, T. Y., Zhu, Y. S., Li, M. R., Shang, D. J., Wang, H. C., Lu, K. D., Guo, S., Zeng,
840 L. M., and Zhang, Y. H.: Aerosol Liquid Water Driven by Anthropogenic Inorganic Salts: Implying
841 Its Key Role in Haze Formation over the North China Plain, *Environ. Sci. Technol. Lett.* , 5, 160-166,
842 2018.

843 Xu, W. Q., Han, T. T., Du, W., Wang, Q. Q., Chen, C., Zhao, J., Zhang, Y. J., Li, J., Fu, P. Q., Wang, Z.
844 F., Worsnop, D. R., and Sun, Y. L.: Effects of Aqueous-Phase and Photochemical Processing on
845 Secondary Organic Aerosol Formation and Evolution in Beijing, China, *Environ. Sci. Technol.*, 51,
846 762-770, 10.1021/acs.est.6b04498, 2017.

847 Zhang, Q., Jimenez, J. L., Canagaratna, M. R., Ulbrich, I. M., Ng, N. L., Worsnop, D. R., and Sun, Y.:
848 Understanding atmospheric organic aerosols via factor analysis of aerosol mass spectrometry: a
849 review, *Anal. Bioanal. Chem.*, 401, 3045-3067, 10.1007/s00216-011-5355-y, 2011.

850 Zhang, Y., Chen, Y. Z., Lambe, A. T., Olson, N. E., Lei, Z. Y., Craig, R. L., Zhang, Z. F., Gold, A., Onasch,
851 T. B., Jayne, J. T., Worsnop, D. R., Gaston, C. J., Thornton, J. A., Vizuete, W., Ault, A. P., and Surratt,
852 J. D.: Effect of the Aerosol-Phase State on Secondary Organic Aerosol Formation from the Reactive
853 Uptake of Isoprene-Derived Epoxydiols (IEPDX), *Environ. Sci. Technol. Lett.* , 5, 167-174, 2018.

854 Zhang, Y. J., Tang, L. L., Croteau, P. L., Favez, O., Sun, Y. L., Canagaratna, M. R., Wang, Z., Couvidat,
855 F., Albinet, A., Zhang, H. L., Sciare, J., Prevot, A. S. H., Jayne, J. T., and Worsnop, D. R.: Field
856 characterization of the PM_{2.5} Aerosol Chemical Speciation Monitor: insights into the composition,

857 sources, and processes of fine particles in eastern China, *Atmos. Chem. Phys.*, 17, 14501-14517,
858 10.5194/acp-17-14501-2017, 2017.

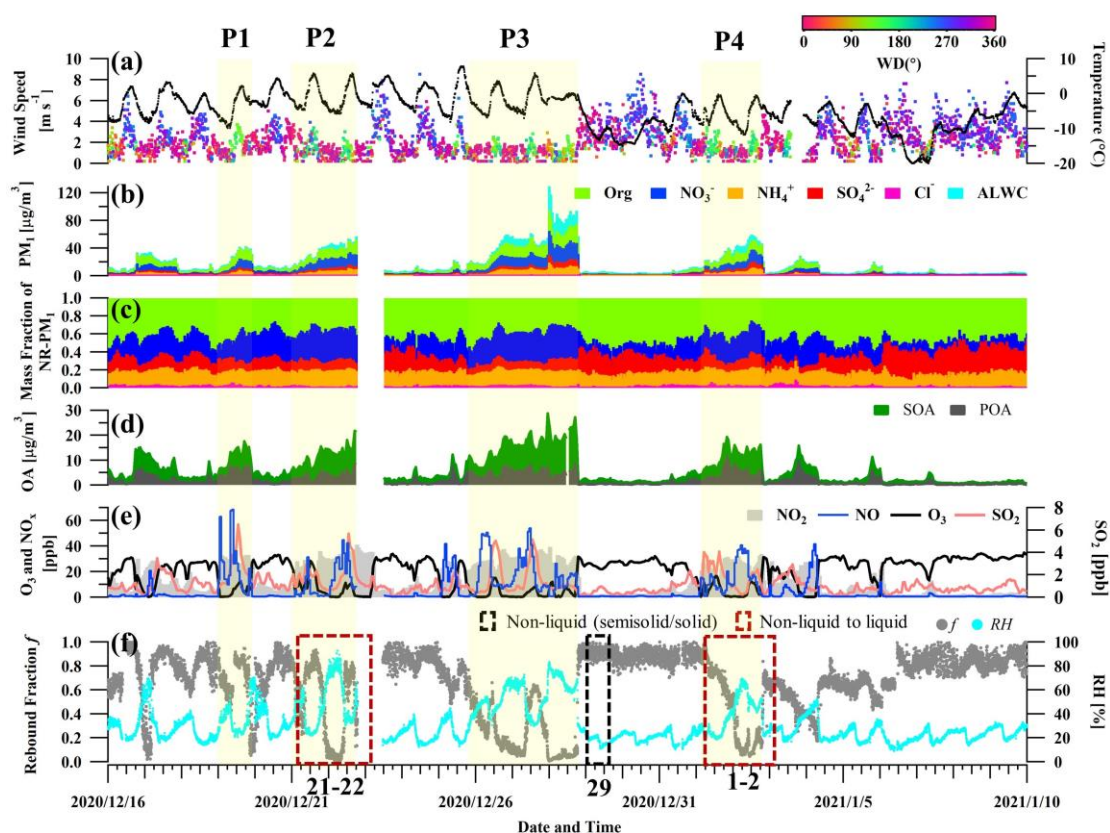
859 Zhao, Z., Xu, Q., Yang, X., and Zhang, H.: Heterogeneous Ozonolysis of Endocyclic Unsaturated
860 Organic Aerosol Proxies: Implications for Criegee Intermediate Dynamics and Later-Generation
861 Reactions, *ACS Earth Space Chem.*, 3, 344-356, 10.1021/acsearthspacechem.8b00177, 2019.

862 Zheng, B., Zhang, Q., Zhang, Y., He, K. B., Wang, K., Zheng, G. J., Duan, F. K., Ma, Y. L., and Kimoto,
863 T.: Heterogeneous chemistry: a mechanism missing in current models to explain secondary
864 inorganic aerosol formation during the January 2013 haze episode in North China, *Atmos. Chem.*
865 *Phys.*, 15, 2031-2049, 10.5194/acp-15-2031-2015, 2015.

866 Zheng, Y., Chen, Q., Cheng, X., Mohr, C., Cai, J., Huang, W., Shrivastava, M., Ye, P., Fu, P., Shi, X.,
867 Ge, Y., Liao, K., Miao, R., Qiu, X., Koenig, T. K., and Chen, S.: Precursors and Pathways Leading to
868 Enhanced Secondary Organic Aerosol Formation during Severe Haze Episodes, *Environ. Sci.*
869 *Technol.*, 55, 15680-15693, 10.1021/acs.est.1c04255, 2021.

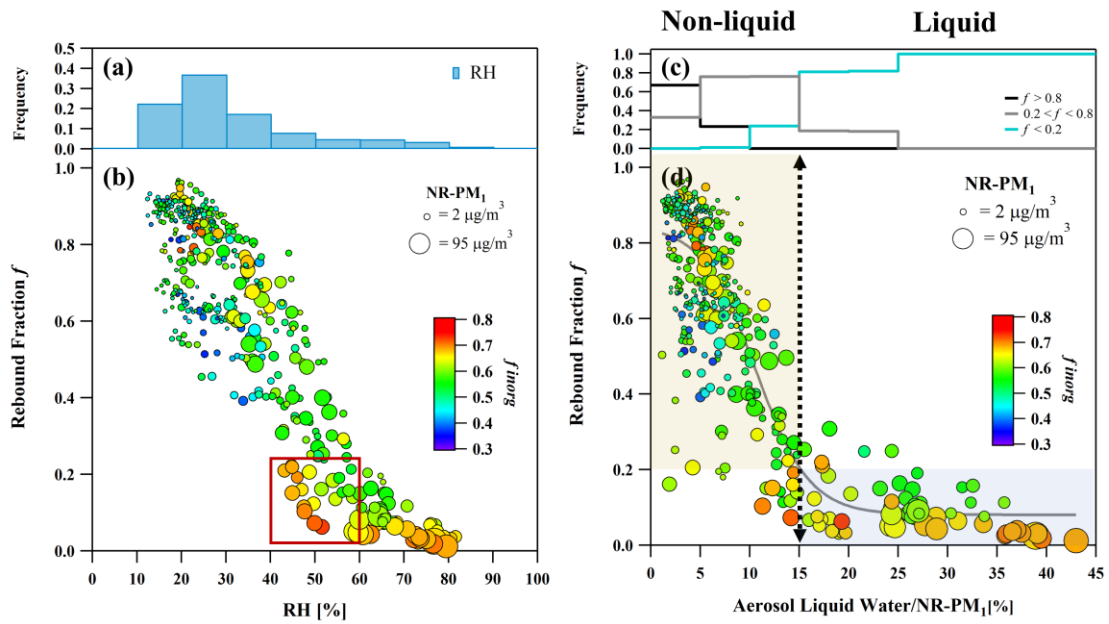
870 Zheng, Y., Miao, R. Q., Zhang, Q., Li, Y. W., Cheng, X., Liao, K. R., Koenig, T. K., Ge, Y. L., Tang, L. Z.,
871 Shang, D. J., Hu, M., Chen, S. Y., and Chen, Q.: Secondary Formation of Submicron and
872 Supermicron Organic and Inorganic Aerosols in a Highly Polluted Urban Area, *J. Geophys. Res.*
873 *Atmos.*, 128, 10.1029/2022jd037865, 2023.

874



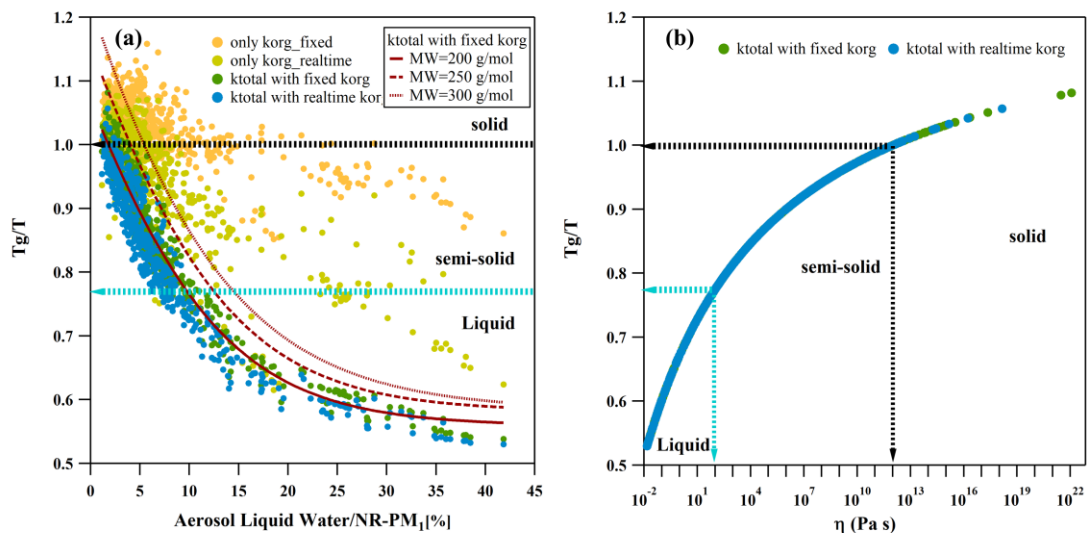
876

877 Figure 1. Time series of (a) wind speed (WS), wind direction (WD) and temperatures,
 878 (b) mass concentration of NR-PM₁ and ALW, (c) mass contribution of NR-PM₁, (d)
 879 mass concentrations of SOA and POA, (e) concentrations of gas pollutants (NO₂, NO,
 880 O₃, and SO₂), (f) rebound fraction and ambient RH during the field campaign. In panel
 881 (f), the black (red) frame with dashed line represents the non-liquid state (transition
 882 from non-liquid to liquid state) of bulk PM_{2.5} droplets based on off-line viscosity
 883 measurement using poke-and-flow technique (Song et al., 2022).



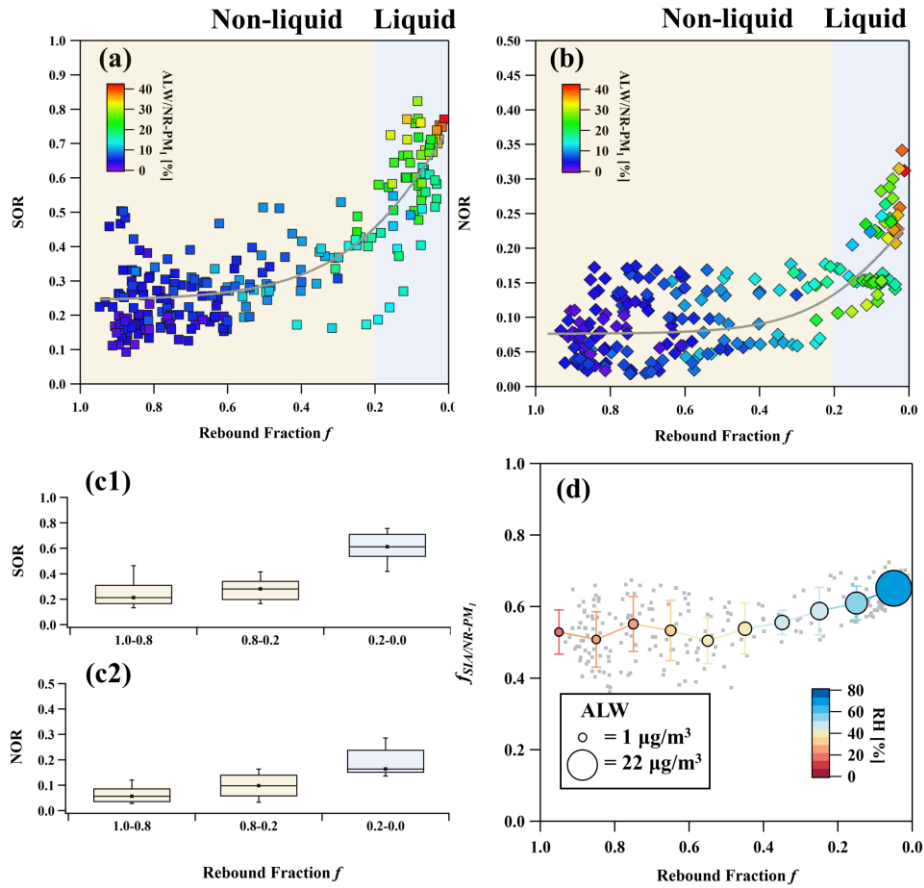
884

885 Figure 2. The frequency distribution of ambient RH in each RH bin (a) and the
 886 frequency distribution of each f interval in each ALW/NR-PM₁ bin (c). Rebound
 887 fraction f as a function of ambient RH (b) and ALW/NR-PM₁ (d) during the observation.
 888 In panel (b) and (d), the scatter points are colored by f_{inorg} in NR-PM₁ and the point size
 889 is scaled by NR-PM₁ mass concentration. The yellow and blue shadow represent the
 890 non-liquid and liquid phase, respectively.



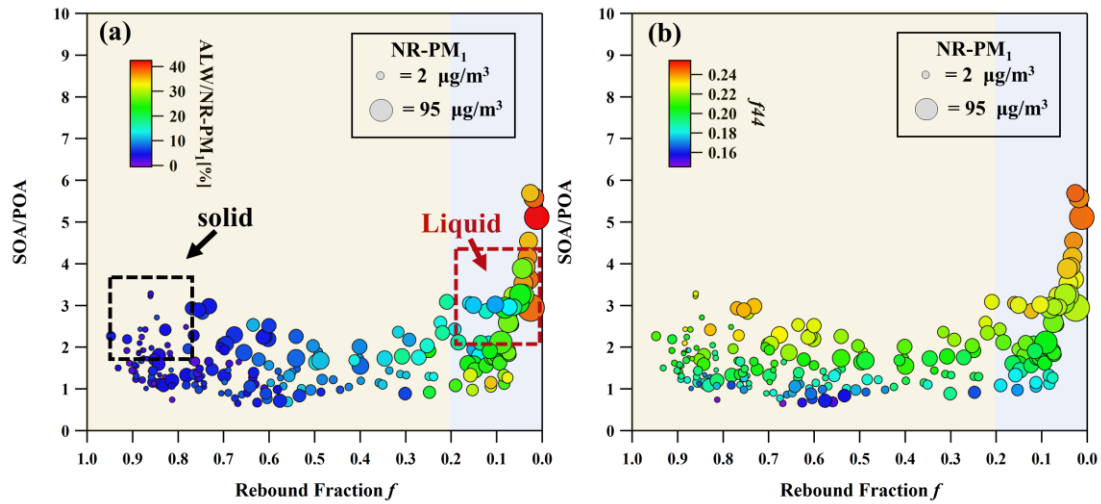
891

892 Figure 3. Characteristic relations between T_g/T and ALW/NR-PM₁ (a) and T_g/T as a
 893 function of predicted viscosity η (b) of organic aerosols under ambient conditions. In
 894 panel (a), the red curves, which employ sigmoid fitting, represent variations in average
 895 molecular weights of OA used for T_g calculation in consideration of the total
 896 hygroscopicity of the particles. The characteristics of the particle-phase state are
 897 delineated by arrows and dashed lines.



898

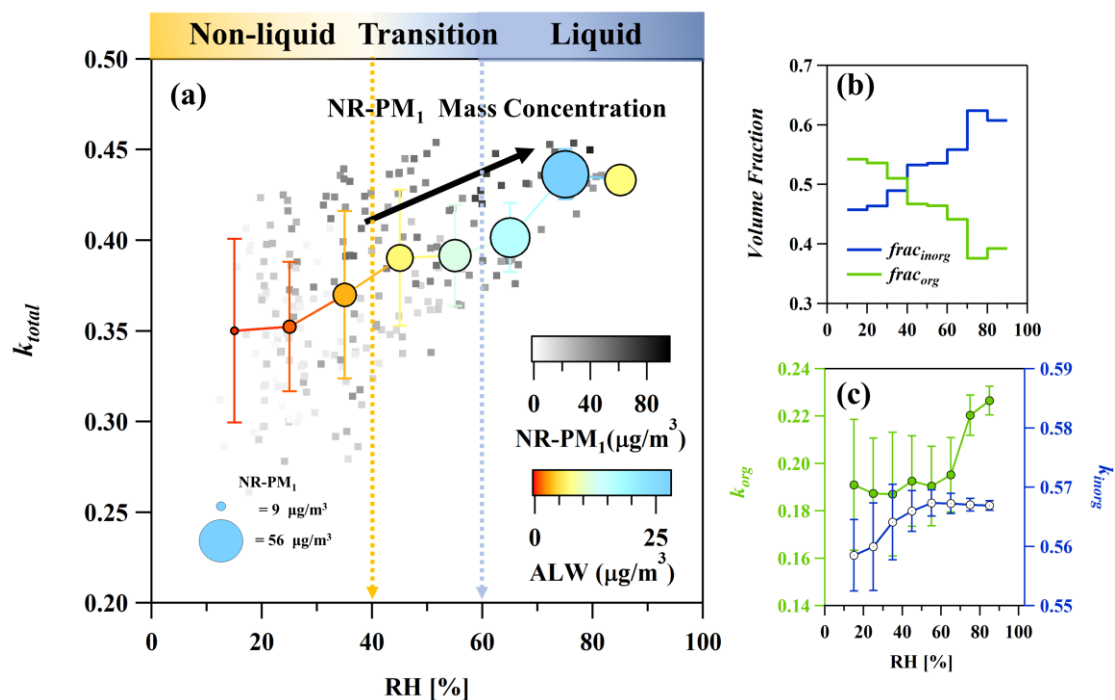
899 Figure 4. SOR and NOR as a function of f (a, b), relationship between SOR or NOR
 900 and three phase transition level (c1, c2), and the mass fraction of SIA in NR-PM₁ as a
 901 function of f during haze episodes (d). Non-liquid particles are marked by yellow
 902 shadows and liquid particles are marked by blue shadows. In panel (a) and (b), the
 903 scatter points are colored by ALW/NR-PM₁ and the trend lines are obtained by sigmoid
 904 fitting. In panel (c1) and (c2), the box plots show 10th, 25th, median, 75th and 90th
 905 percentiles. In panel (d), RH is indicated by color, and ALW mass concentration is
 906 indicated by the size of the circle. The error bars show one standard deviation.



907

908 Figure 5. The relationship between SOA/POA and particle rebound fraction f for phase
 909 transition (a) and oxidation degree (b) during haze episodes. Non-liquid particles are
 910 marked by yellow shadows and liquid particles are marked by blue shadows. The circles
 911 are colored by $ALW/NR-PM_{10}$ and f_{44} to represent water uptake capacity and particle
 912 oxidation degree in panel (a) and panel (b), respectively. The sizes of the circles are
 913 scaled to $NR-PM_{10}$ mass concentrations. The black (red) frame with dashed line
 914 represent the off-line viscosity measurement results using poke-and-flow technique
 915 corresponding to Figure 1.

916



917

918 Figure 6. The overall hygroscopicity of particles (a), average volume fraction (b) and
 919 hygroscopicity (c) of inorganics and organics as a function of RH during haze episodes.
 920 k_{total} was calculated using real-time k_{org} . Particles in different phase state condition,
 921 including non-liquid, phase transition from non-liquid to liquid, and liquid, are visually
 922 distinguished through a gradual color change from yellow to blue, which correlates with
 923 RH. In panel (a), the scatter points are colored by NR-PM₁ mass concentrations and
 924 averaged in each RH bin. Averaged ALW and NR-PM₁ mass concentrations are
 925 indicated by color and the size of the circle, respectively. The error bars show one
 926 standard deviation.